Antenna Sensor for Radio-wave-type Endoscope

Takafumi Fujimoto,* Keiya Kawashima, Genki Horiguchi, and Toshiyuki Tanaka

Graduate School of Engineering, Nagasaki University,
1-14 Bunkyo, Nagasaki 852-8521, Japan

In this paper, an antenna sensor for a radio-wave-type endoscope to detect a blood vessel in fatty tissue is proposed. The antenna sensor consists of one transmitting antenna and two receiving antennas. As the antenna element, microstrip antennas are used. The relationships between the antenna arrangement and the magnitude of the reflected wave from the blood vessel are discussed using a 2.5-times scale simulation model. In the simulation, it is confirmed that the blood vessel of 10 mm diameter can be detected at a distance of 10 mm from the top surface of the fatty tissue in the 2.5-times scale model using the proposed antenna sensor.

1. Introduction

Recently, endoscopes have been used in many surgical operations. In endoscopic surgery, holes are bored in the abdomen to permit the insertion of the endoscopes and surgical instruments. However, the holes are very small. Therefore, endoscopic surgery has some great advantages. One of them is that the postoperative pain is minimal and another is that the wound heals faster than in the case of an abdominal operation. However, endoscopic surgery has a major drawback. In many cases, the fatty tissue attached to the surface of the viscera covers the blood vessels on the viscera. Therefore, the surgeon must remove the fatty tissue first in the endoscopic operation. In the surgical operation, the ultrasonic inspection device is used to detect the position of the blood vessel. In the endoscopic operation, however, as the abdominal cavity is filled with carbon dioxide, it is impossible to obtain a supersonic wave image using only a supersonic wave probe on the surface of a body.[1] Although an endoscope using supersonic waves has been developed recently,[1,2] it is not used to detect the blood vessels behind fatty tissue. In the present endoscopic surgery, an infrared laser is used to detect the blood vessels behind the fatty tissue. However, the infrared laser is greatly affected by the fatty tissue.[3] The detectable depth for blood vessels seems to be around 2 mm from the surface of the fatty tissue. In current endoscopic surgery, there is a risk of damaging the blood vessels. Under such conditions, a new instrument for detecting blood vessels behind the fatty tissue is required.

Generally, the propagation loss of the radio wave is small compared with that of the infrared ray. Therefore, an endoscope using radio waves has the possibility of detecting the blood vessel deep into the fatty tissue, which is impossible with the infrared laser endoscope. An endoscope using radio waves has not yet been proposed. The aim of this study is the development of an endoscope that can project an image of a blood vessel using radio waves in real time. Therefore, as a sensor for detecting the blood vessel, antennas are used. The proposed antenna sensor consists of one transmitting antenna and multiple receiving antennas. The position of the blood vessel is detected by processing the signal of the received radio wave into image data. Generally, antennas for wideband operation, such as a Vivaldi antenna[4] and a bowtie antenna,[5] are used for buried-object detection. In the endoscope, however, the area where the antennas are installed is very small. Moreover, multiple antenna elements must be installed. Therefore, although the impedance bandwidth is narrow, a microstrip antenna (MSA)[6] is adopted as the antenna element because of its low profile and easy miniaturization. In this work, the possibility of the proposed antenna sensor is investigated by examining the simulated transmitting coefficients in both the frequency and time domains.

2.　Specification of Endoscope in a 2.5-times Scale Model

In blood vessel detection, the resolving power must be maintained over a depth of approximately 2–5 mm from the top surface of the fatty tissue to the blood vessel. As the frequency increases, the resolving power of the radio wave also increases. Generally, the resolving power is a fraction of the wavelength. At 10 GHz, the wavelength in the fatty tissue (relative permittivity $\cong 4$) is 15 mm. Therefore, a frequency higher than 10 GHz is suitable to obtain the required resolving power. However, as the frequency increases, the attenuation of the radio wave in the fatty tissue also increases. In this sensor, therefore, it is planned to use microwave in the frequency range from the 15 to 25 GHz band. The diameter of the practical endoscope is very small (less than 10 mm). In the proposed antenna sensor, multiple antennas must be arranged in a small area. Therefore, as the first step of our study, a 2.5-times scale model of the proposed sensor is examined to facilitate the fabrication and measurement of the antenna sensor. The frequency range from 15 to 25 GHz corresponds to the frequency range from 6 to 10 GHz in the 2.5-times scale model.

Figure 1 shows the analytical model. The transmitting and receiving antennas are located on top of the fatty tissue and face towards both the fatty tissue and the blood vessel. The dimensions of the fatty tissue are $W_f \times L_f \times D_f$. The diameter of the blood vessel is d_b. The distance between the top of the blood vessel and the top surface of the fatty tissue is h_b. Although the thickness of the fatty tissue depends on the person, D_f is set to 50 mm in this paper. The dimensions of the fatty tissue are also set to $W_f \times L_f = 200 \times 200$ mm^2.

Table 1 shows the actual diameter d_b and the distance h_b, and d_b and h_b of the 2.5-times scale model. Sinclair proposed the theory of a scaling model and derived the scale factors in nondispersive media.[7] According to Sinclair's theory, the relative permittivity and conductivity must also be transformed by the scaling factor. However, as the fatty tissue and blood vessels are dispersive media, Sinclair's theory cannot be used in this study. Figures 2(a)
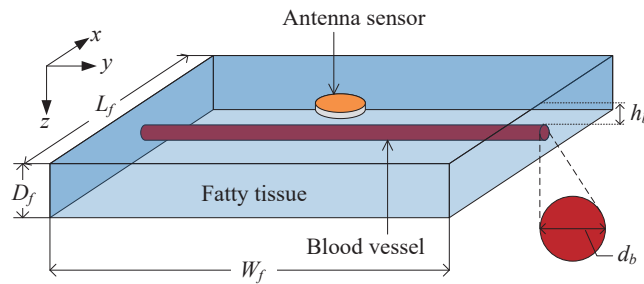
Fig. 1.   (Color online) Analytical model.

Table 1
Diameter and location of the blood vessel.

	Diameter d_b (mm)	Distance h_b (mm)
Actual values	4–8	2–8
2.5-times scale model	10–20	5–20

(a)

(b)
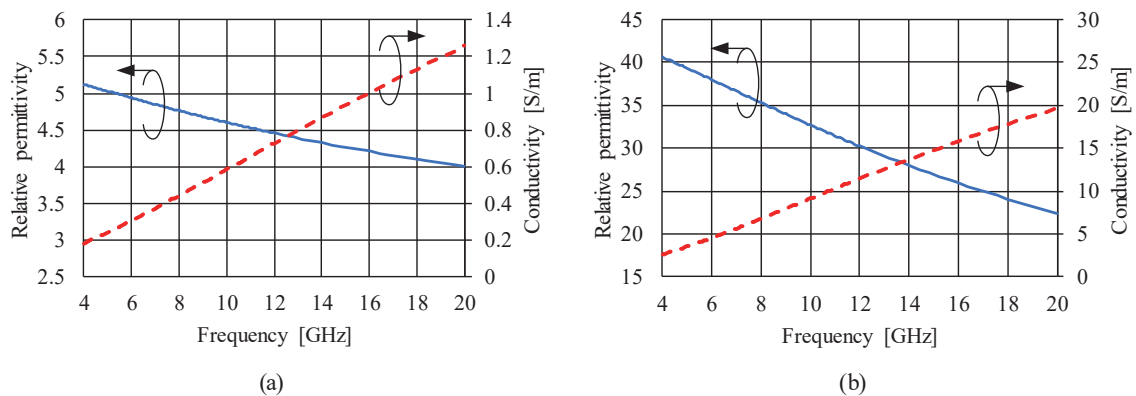
Fig. 2.   (Color online) Frequency characteristics of (a) fatty tissue and (b) blood vessel.

and 2(b) show the relative permittivities and conductivities of the fatty tissue and blood vessel including blood, respectively.[8] As the frequency increases, the conductivity increases and the attenuation of the radio wave propagating in the fatty tissue becomes large. The attenuation affects the reception of the reflected wave from the blood vessel. In dispersive media, therefore, the relative permittivity and conductivity in the scale model should be designed in consideration of the attenuation. Figures 3(a) and 3(b) show the magnitude of the plane wave for various depths of the fatty tissue and the blood vessel, respectively. The distances of the propagation in Figs. 3(a) and 3(b) correspond to the thicknesses of the fatty tissue and the blood vessel, respectively. The equation of the magnitude in the plane wave is expressed as
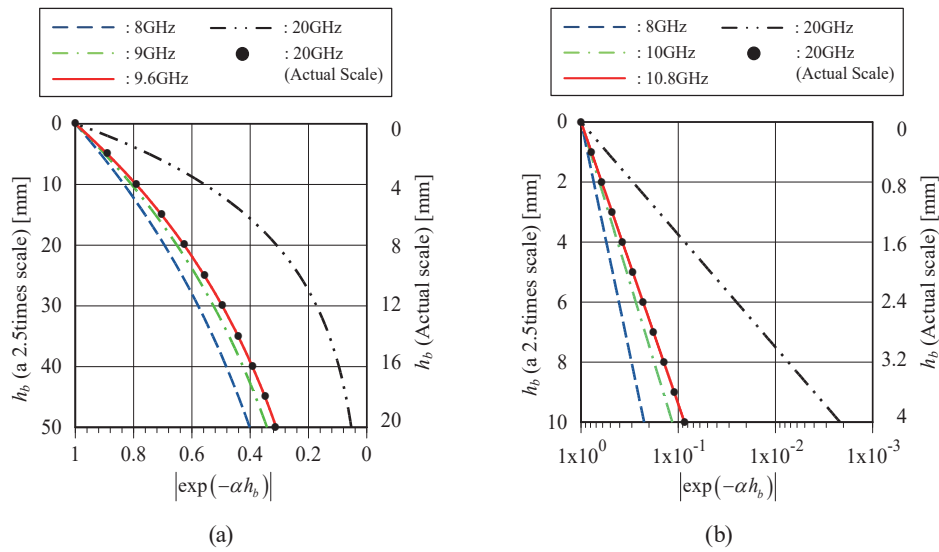
Fig. 3.   (Color online) Attenuation characteristics of plane waves in (a) fatty tissue and (b) blood vessel.

$$\left| \exp(-\alpha h_b) \right|, \quad \alpha = \mathrm{Im}\left(k_0 \sqrt{\varepsilon_r + \frac{\sigma}{j\omega\varepsilon_0}} \right), \tag{1}$$

where k_0 and ε_0 are the wave number and the permittivity in free space, respectively. ω is the angular frequency. ε_r and σ are the relative permittivity and conductivity, respectively. The magnitude of the plane wave at 9.6 GHz in the 2.5-times scale model is very similar to that at 20 GHz in the actual scale model. Therefore, the relative permittivity and conductivity of the fatty tissue at 9.6 GHz are used in this study. Similarly, the relative permittivity and conductivity of the blood vessel are determined. In the blood vessel, those at 10.8 GHz are used. The relative permittivity and conductivity of the fatty tissue are 4.633 and 0.5566 S/m at 9.6 GHz, respectively. Those of the blood vessel are 31.67 and 10.07 S/m at 10.8 GHz, respectively.

Actually, viscera exist under the fatty tissue. However, the attenuation of microwaves is large in the fatty tissue because the conductivity of the fatty tissue is relatively high (conductivity = 0.5566 S/m). Since the magnitude of the reflected wave from the interface between the fatty tissue and the viscera is small, the viscera is not considered in the analytical model.

3.   Antenna Design

To investigate the antenna arrangement method, the structure of the antennas in Fig. 4 is analyzed. The antenna element #1 for transmission is located at the center and the four surrounding antenna elements #2–#5 are for reception. Rectangular MSA is used for the antenna elements. The antenna size is adjusted so that the center frequency becomes approximately 8 GHz. The size of all the antenna elements is the same, $L_a \times W_a = 7.70 \times 3.0$ mm^2. Antenna elements #2 and #4 are arranged in parallel to antenna
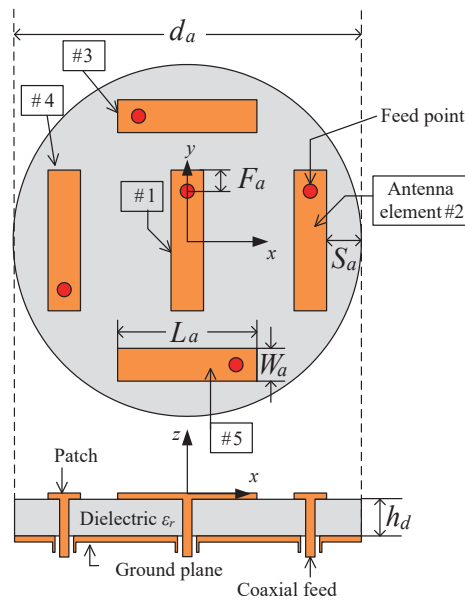
Fig. 4.   (Color online) Geometry of antenna.

element #1, and antenna elements #3 and #5 are arranged perpendicular to antenna element #1. The antennas are fed by a coaxial feed through the dielectric substrate from the ground plane. The ground planes of all the antenna elements are shared. The impedance matching of the MSA is tuned in accordance with the position of the feed point. The feed point in antenna #1 is on the positive y-axis. Although the feed point in antenna #2 is also located on the positive y-axis, that in antenna #4 is located on the negative y-axis. The feed points of antennas #3 and #5 are also located at the sides opposite to each other's origin on the x-axis. The diameter of the antenna, d_a, is 25 mm. The thickness of the dielectric substrate is $h_d = 3.2$ mm. Its relative permittivity and dielectric loss tangent are $\varepsilon_r = 3.8$ and $\tan \delta = 0.022$, respectively.

In this work, two study cases of the positional relationship between the transmitting antenna and the blood vessel are examined. Figure 5 shows the two cases, A and B. In case A, the blood vessel is located parallel to transmitting antenna #1. In case B, the blood vessel is located perpendicular to transmitting antenna #1.

4.   Results and Discussion

For the calculations in this study, the simulation software package XFDTD version 7.6,[9] which is based on the finite difference time domain method, is used. In the simulation software, a perfectly matched layer (PML) with 7 layers is used as the boundary condition surrounding the analytical space. The sizes of the cell along the x-, y-, and z-axes are the same, from 0.097 to 0.92 mm.

In this paper, the transmission coefficients determined by the simulation are discussed. In the experiment, they can be measured using the network analyzer. As the network analyzer has the dynamic range of 100 dB, the reception level from the blood vessel is set to −60 dB.
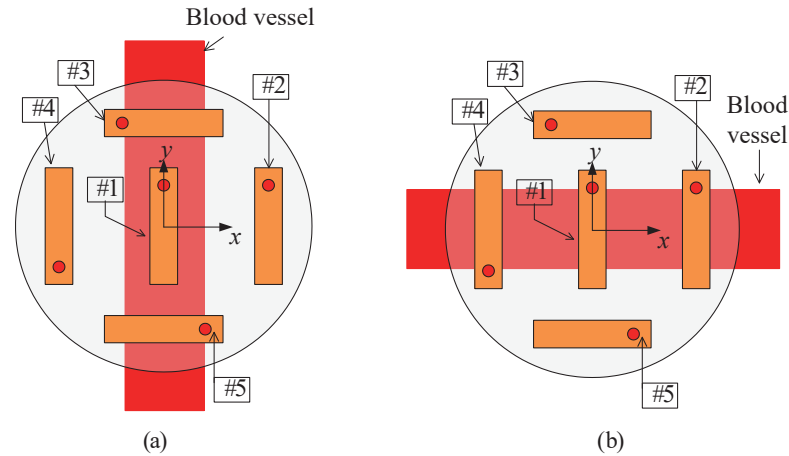
Fig. 5.   (Color online) Positional relationships between antennas and blood vessel. (a) Case A and (b) case B.

4.1   Analysis in frequency domain

Antennas for communication in the far field are designed so that the magnitude of the reflection coefficient is less than or equal to −10 dB. Although the antennas are used in the near-field region in this study, the reflection coefficient should be as small as possible to receive the signals with the slight reflection from the blood vessel. Figure 6 shows the simulated reflection coefficient $|Snn|$ (n = 1, 2, 3, 4, and 5) in the case with the fatty tissue, but without the blood vessel. In the MSAs, the input impedance around the resonant frequency can generally be adjusted by changing the position of the feeding point. In this analytical model, however, the input reactance is around 50 Ω because of the existing fatty tissue and the many feeding pins. Therefore, the minimum reflection coefficients of the optimized antennas are from around −6 to −9 dB at 8.0 GHz. In this study, therefore, the reflection coefficient is set to −5 dB.

Figure 7 shows the transmission coefficients $|Sm1|$ (m = 2, 3, 4, and 5) in case A. d_b is 10 mm and h_b is from 5.0 to 12.5 mm. In the case without the blood vessel, the magnitudes of the transmitting coefficient of all the receiving antennas are from −25 to −30 dB around 8 GHz. Regardless of the direction of the antennas, the mutual couplings between the transmitting and receiving antennas are at the same level. The differences in $|S21|$ and $|S41|$ between the presence and absence of the blood vessel are observed from 6 to 12 GHz. However, the differences in $|S31|$ and $|S51|$ are very small for the following reason. The electric current on the transmitting antenna flows strongly along the y-axis. Therefore, the y-component of the electric near field is greater than its x-component. Therefore, the y-component is produced strongly in the reflected wave from the blood vessel. The direction of receiving antennas #2 and #4 is the same as that of transmitting antenna #1; however, the direction of antennas #3 and #5 is perpendicular to that of antenna #1. Therefore, antennas #2 and #4 are excited strongly by the y-component of the electric field reflected from the blood vessel compared with antennas #3 and #5. It is found that although the antennas in this sensor are used in the near-field region, the antennas must be arranged in consideration of the relationships among the directions of the transmitting and
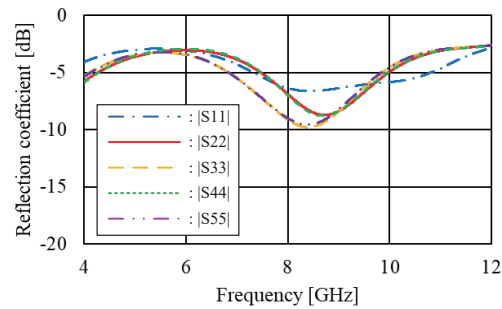
Fig. 6.   (Color online) Simulated reflection coefficients.
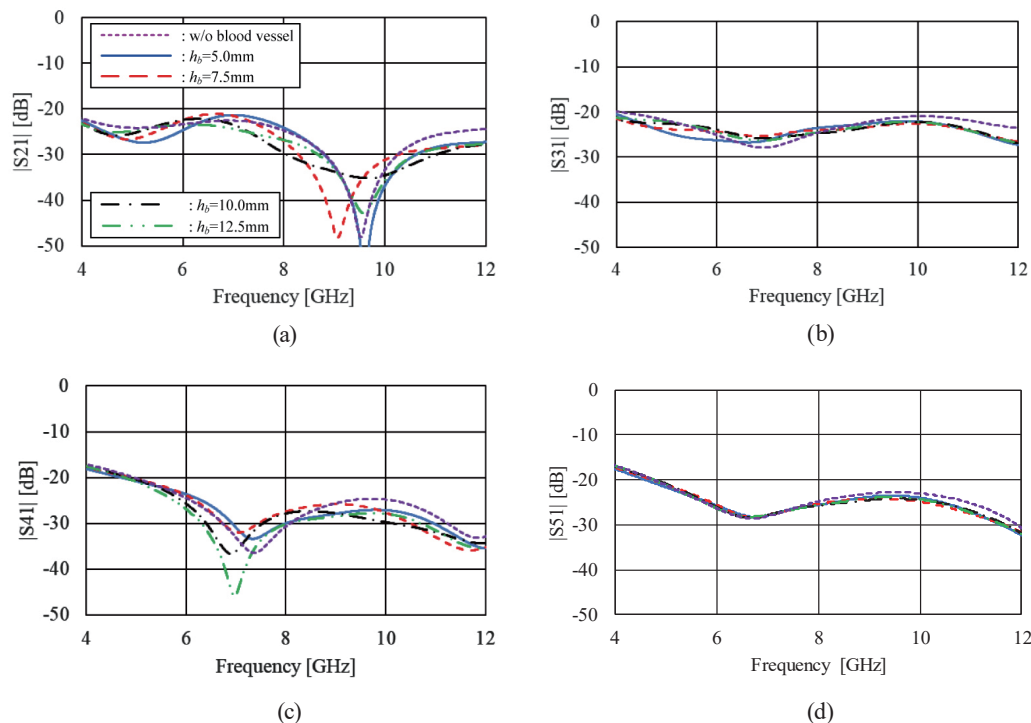
Fig. 7.   (Color online) Simulated transmission coefficients in case A. (a) $|S21|$, (b) $|S31|$, (c) $|S41|$, and (d) $|S51|$.

receiving antennas. Although antennas #2 and #4 are located symmetrically to antenna #1, the position of the feed point in antenna #2 is different from that in antenna #4. Therefore, $|S21|$ is also different from $|S41|$.

Figure 8 shows the transmission coefficients $|Sm1|$ (m = 2, 3, 4, and 5) in case B. Similar to case A in Fig. 7, the differences between the presence and absence of the blood vessel in $|S21|$ and $|S41|$ are observed from around 6 to 12 GHz. Since the tendencies in cases A and B are the same, the simulated results for case B will be omitted hereafter.
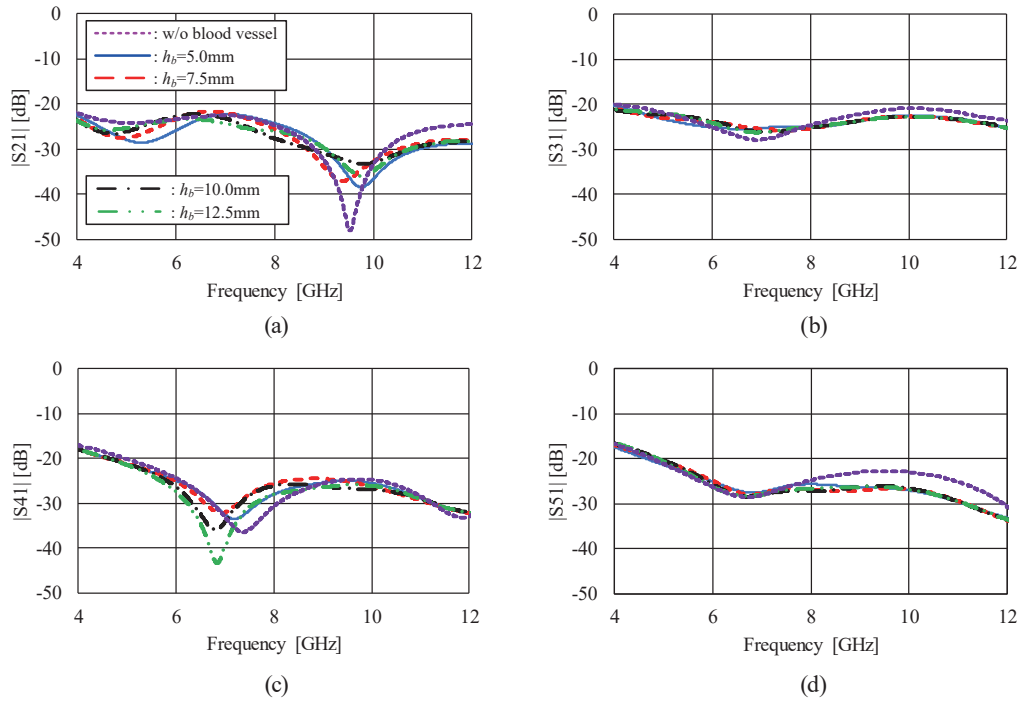
Fig. 8.   (Color online) Simulated transmission coefficients in case B. (a) |*S*21|, (b) |*S*31|, (c) |*S*41|, and (d) |*S*51|.

    Figure 9 shows the magnitude of the electric field distribution within the fatty tissue ($z = 5$ mm) at the *xy*-plane in the case without the blood vessel. The time is 0.3 ns and frequency is 8.0 GHz. Although the electric field in the vicinity of the feed pin of the transmitting antenna is strong, the electric field in the vicinity of all the receiving antennas is uniformly distributed.

    Figures 10(a) and 10(b) show the magnitude of the electric field distributions within the fatty tissue in the case with the blood vessel in the *xz*- and *yz*-planes. The blood vessel is located at $h_b = 5$ mm along the *y*-axis (Case A). The frequency is 8 GHz and time is 0.3 ns. It can be observed that the radiated electric field is attenuated by the blood vessel, and the magnitude of the electric field under the blood vessel decreases.

4.2   Analysis in time domain

    The waveforms in the frequency domain are processed by inverse Fourier transform to obtain the waveforms in the time domain. Inverse Fourier transform is expressed using the following equations.

$$f(t) = \int_{-\infty}^{\infty} F(f) e^{j2\pi ft} df \tag{2}$$

$$F(f) = G(f) P(f) H(f) \tag{3}$$
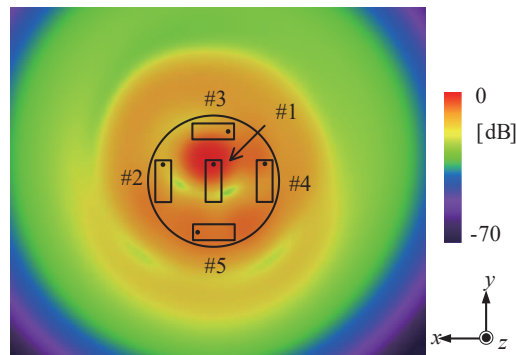
Fig. 9.   (Color) Simulated electric field distribution without blood vessel in *xy*-plane.

(a)

(b)
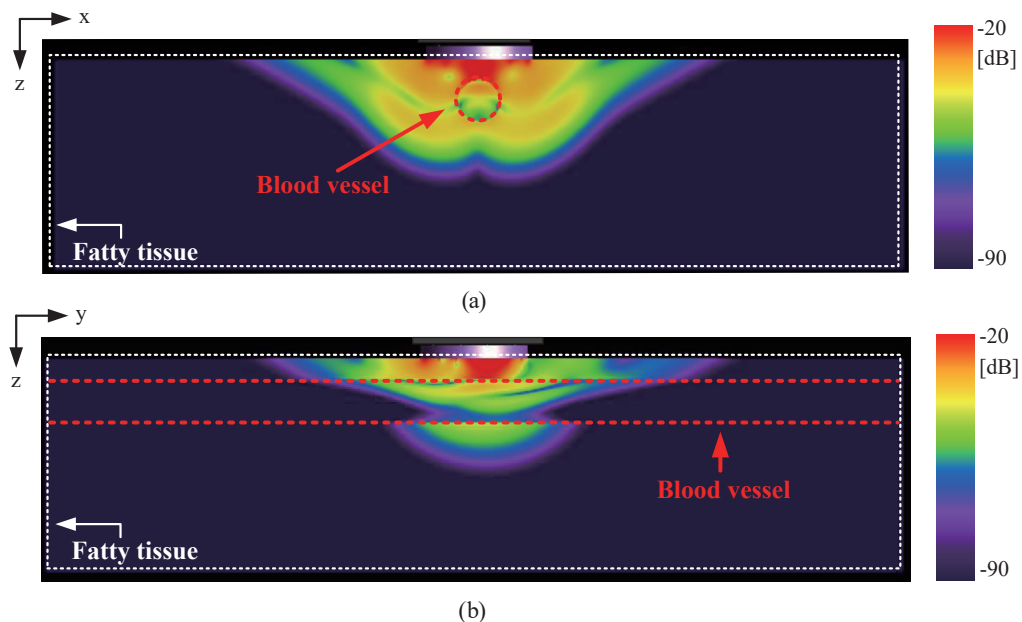
Fig. 10.   (Color) Simulated electric field distribution with blood vessel. (a) *xz*- and (b) *yz*-planes.

where *f* and *t* are frequency and time, respectively. $G(f)$ is the simulated data in the frequency domain, $P(f)$ is a weight function, and $H(f)$ is a rectangular window function that is zero-valued beyond 25 GHz. The third derivative of the Gaussian function with the center frequency of 8.0 GHz is used for $P(f)$.

Figures 11(a)–11(d) show the amplitudes of the transmission coefficients $Sm1$ ($m = 2, 3, 4,$ and 5) in the time domain in case A. In the amplitude with respect to $S21$ and $S41$, the differences between the cases with the blood vessel from $h_b = 5.0$ to 12.5 mm and the case without the blood vessel are observed from $t = 0.25$ to 0.45 ns. Figures 12(a) and 12(b) are the enlarged figures of the time range from 0.25 to 0.45 ns in Figs. 11(a) and 11(c), respectively. As the distance of propagation increases, the arrival time of the radio wave becomes late. In both $S21$ and $S41$, the regularity of the arrival time can be observed in the reflected waves from the blood vessel at the
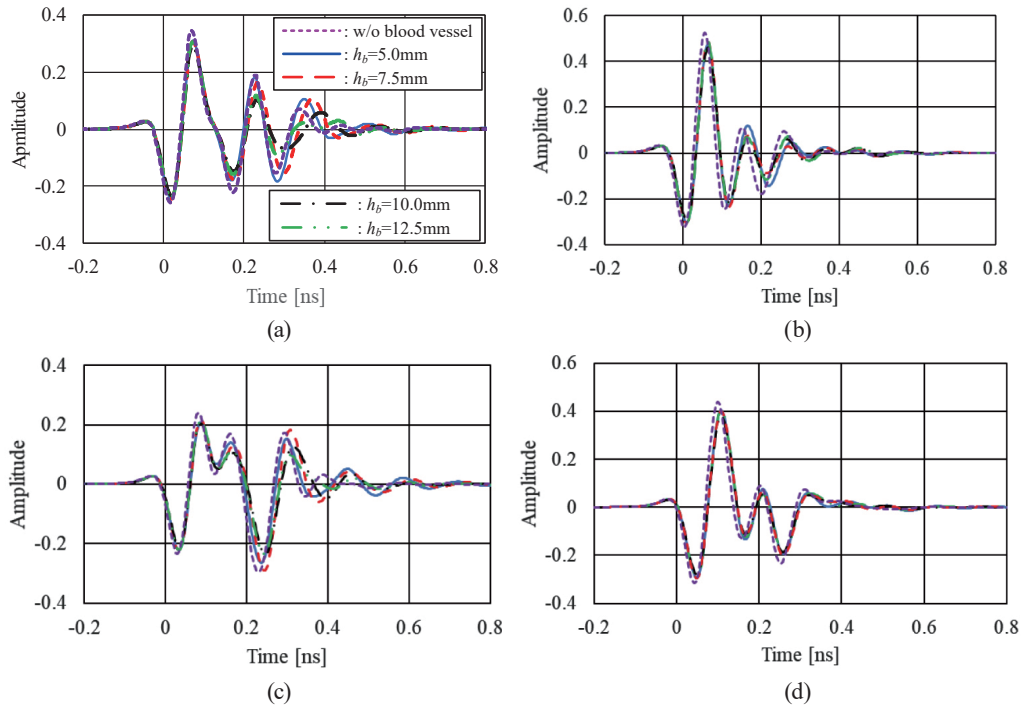
Fig. 11.   (Color online) Simulated transmission coefficients in time domain. (a) $S21$, (b) $S31$, (c) $S41$, and (d) $S51$.
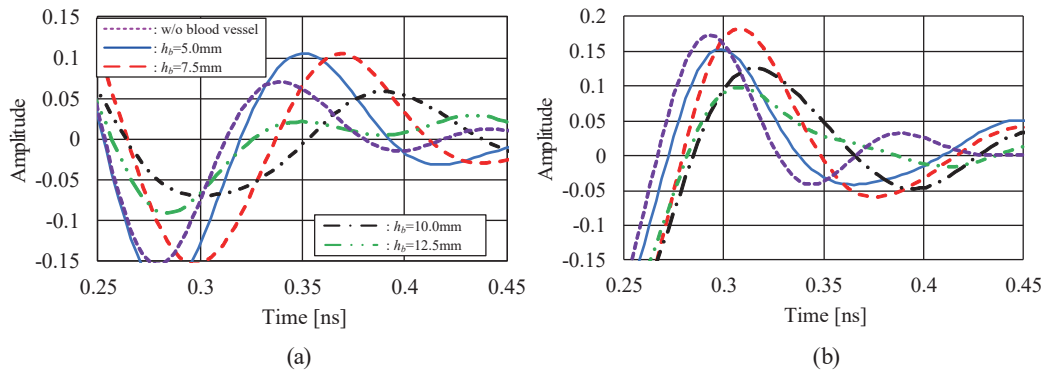
Fig. 12.   (Color online) Enlargement of Figs. 11(a) and 11(c). (a) $S21$ and (b) $S41$.

depth from $h_b = 5.0$ to 10.0 mm. In the amplitudes with respect to $S31$ and $S51$, the differences depending on h_b are not obvious. In the time domain, it is also confirmed that the antennas must be arranged in consideration of the polarization plane.

Generally, it is required that the bandwidth of the weight function with a magnitude of −3 dB be included in the impedance bandwidth of the antenna. As shown in Fig. 6, in the proposed antenna, the bandwidth of the −5 dB reflection coefficient is approximately from 7 to 11 GHz. The impedance bandwidth of the antenna corresponds to the frequency range where the magnitude of the third derivative of the Gaussian function with the center frequency of 8.0 GHz becomes −1 dB. In order to satisfy the condition of the bandwidth of the weight function, the

higher derivate should be applied. However, although the weight function does not satisfy the impedance bandwidth of the antenna, it is confirmed in Fig. 12 that the presence of the blood vessel can be observed. A detailed discussion of the relationships between the bandwidth of the weight function and the accuracy of blood vessel detection is needed. This is one of our future tasks.

The transmission coefficients in Figs. 11 and 12 include the following four waves:

(1) the reflected wave from the side surface of the fatty tissue,

(2) the reflected wave from the bottom surface of the fatty tissue,

(3) the direct wave from the transmitting antenna, and

(4) the reflected wave from the blood vessel.

Figure 13 shows the four waves. In order to evaluate the reflected wave from the blood vessel, subtraction processing is applied to the transmission coefficients. Figure 14 shows the concept of subtraction processing. To remove the reflected wave from the bottom surface of the fatty tissue, the thickness of the fatty tissue is extended from $D_f = 50$ to 300 mm. By subtracting the simulated values of the extended model without the blood vessel from those with the blood vessel, the reflected wave from only the blood vessel can be obtained, as shown in Fig. 14.

The differences between the cases with the blood vessel from $h_b = 5.0$ to 12.5 mm and the case without the blood vessel are shown in Figs. 11 and 12. Therefore, subtraction processing
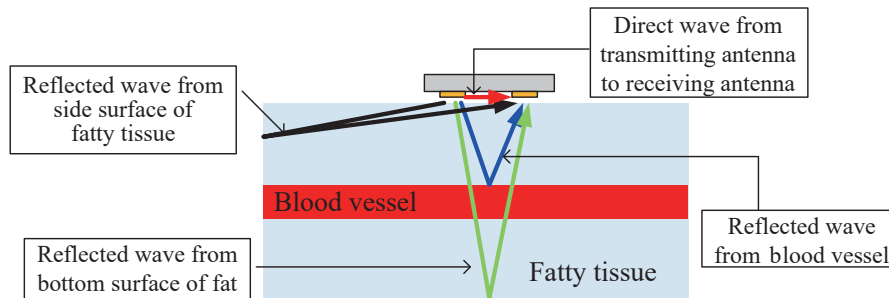
Fig. 13. (Color online) Four kinds of radio waves included in simulated transmission coefficients.
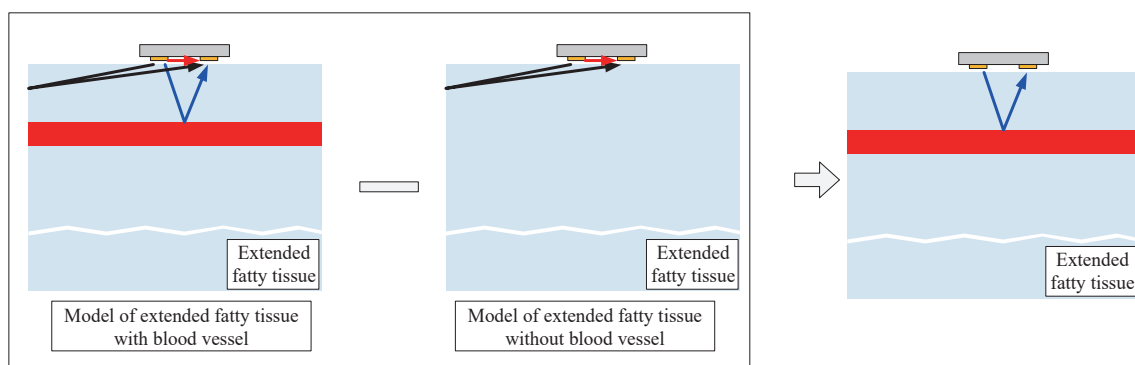
Fig. 14. (Color online) Concept of subtraction processing.

is applied to *S*21 and *S*41. Figures 15(a) and 15(b) show the simulated results obtained by subtraction processing. Regardless of the distance h_b, the same waveform occurs from 0.0 to 0.1 ns. The waveform from 0.0 to 0.1 ns corresponds to the direct wave from the transmitting antenna. Since impedance matching in the case with the blood vessel is different from that without the blood vessel, the magnitudes of the radiated electric field are also different in the cases with and without the blood vessel. In subtraction processing, therefore, the direct wave from the transmitting antenna could not have been subtracted completely. Similar to Figs. 11(a) and 11(b), the differences depending on h_b are observed in the time range from 0.25 to 0.45 ns in Figs. 15(a) and 15(b). Figures 16(a) and 16(b) are the enlarged figures of the time range from 0.25 to 0.5 ns in Figs. 15(a) and 15(b), respectively. In both *S*21 and *S*41, as h_b becomes longer, the arrival time becomes late. This characteristic of the arrival time is the same as that of the transmission coefficients shown in Figs. 11(a) and 11(b). In the time range from 0.35 to 0.45 ns, the maximum amplitudes of *S*21 are 0.052 in h_b = 5.0 mm and 0.95 in h_b = 7.5 mm. Although the blood vessel is shallower at h_b = 5.0 mm than at h_b = 7.5 mm, the maximum amplitude is smaller in h_b = 5.0 mm than in h_b = 7.5 mm. However, the maximum amplitude (0.03) is smaller in h_b = 12.5 mm than in h_b = 7.5 mm. These are due to the following reason. As the position of the blood vessel becomes shallow, the incidence angle from the transmitting antenna to the blood vessel and the reflection angle from the blood vessel to the receiving antenna become

(a)

(b)
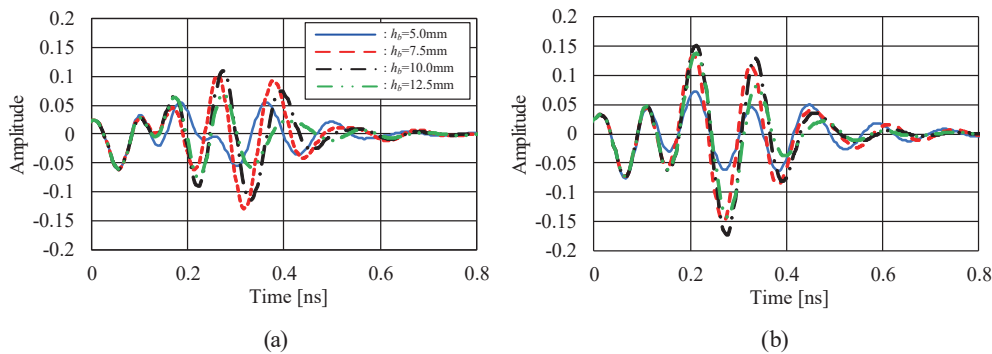
Fig. 15. (Color online) Reflected waves from blood vessel in time domain. (a) *S*21 and (b) *S*41.

(a)

(b)
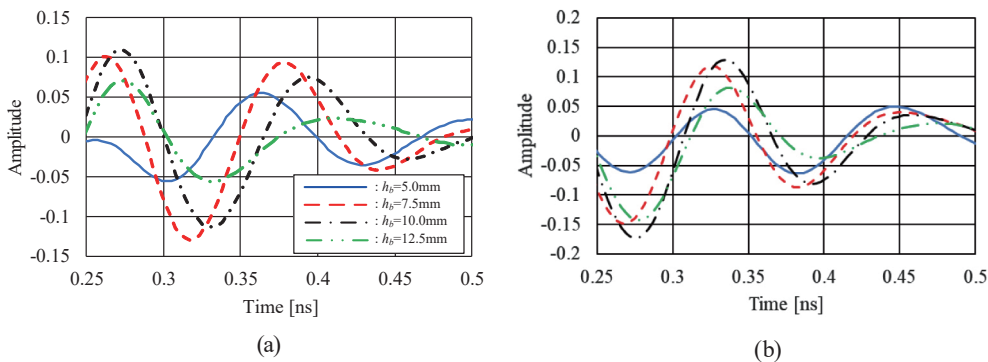
Fig. 16. (Color online) Enlargements of Figs. 15(a) and 15(b). (a) *S*21 and (b) *S*41.

wide. As these angles become wide, the amount of reflection by the blood vessel decreases. However, as the position of the blood vessel is deep, the amount of attenuation due to tan δ of the fatty tissue increases. In $S21$, therefore, the maximum amplitude in $h_b = 7.5$ mm is the largest.

Next, the amplitude of the transmission coefficients in the case that the antennas are moved in the vicinity of the blood vessel is investigated. Figure 17 shows the positional relationship between the directions of the movements of the antenna and the blood vessel. The blood vessel exists between $x = -5$ and $+5$ mm. The antenna sensor moves perpendicular to the blood vessel.

Figure 18 shows the simulated amplitudes of the transmission coefficients in the case that the antennas are moved from $x = -20$ to $+20$ mm. The distance of the blood vessel is $h_b = 5$ mm. In Fig. 18, the amplitudes between -0.25 and 0.25 are shown in a color gradation image and the others are shown in black. In $S21$, the reflected wave can be confirmed at around $t = 0.25$ ns and from $x = -6$ to $+9$ mm. In $S41$, it can be confirmed at around $t = 0.3$ ns and from $x = -12$ to 0 mm. Although the blood vessel can be detected, the positions of the blood vessel obtained by the reflected wave deviate from the actual position in both $S21$ and $S41$. In $S41$, moreover,
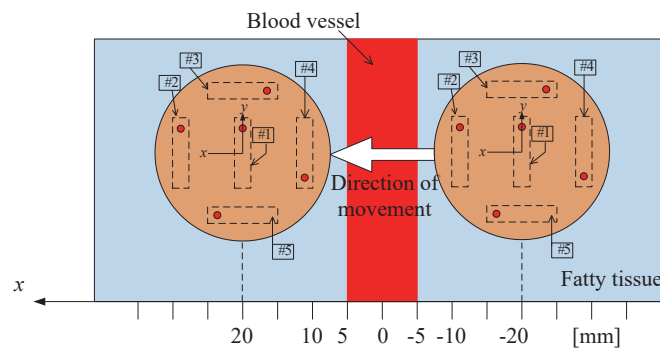
Fig. 17. (Color) Positional relationships between the directions of the movements of the antenna and the blood vessel.
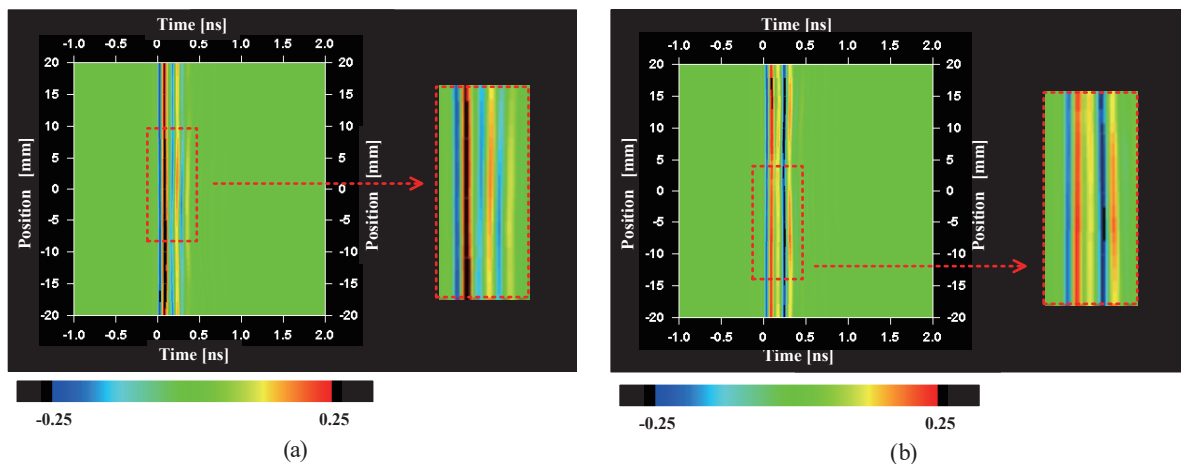
Fig. 18. (Color) Simulated amplitudes of transmission coefficients when the antenna sensor is moved from $x = -20$ to $+20$ mm ($h_b = 5$ mm). (a) $|S21|$ and (b) $|S41|$.

the virtual image appears at around $x = +8$ to $+18$ mm. In $S31$ and $S51$, the reflected wave from the blood vessel cannot be observed. Therefore, $S31$ and $S51$, in the case that the antennas are moved, are omitted in this paper.

4.3 3-element model

From the above simulated results, the receiving antennas should be arranged so that their directions are the same as that of the transmitting antenna. The positions of the blood vessel obtained from the reflected wave shift from the actual position in both $S21$ and $S41$. The direction of the shift depends on the position of the receiving antennas. Therefore, it is expected that the position of the image of the blood vessel can be improved by feeding receiving antennas #2 and #4 at the same edge side and averaging the amplitudes of the reflected waves with respect to $S21$ and $S41$.

Figure 19 shows the final antenna sensor designed in consideration of the above conditions. The receiving antennas #3 and #5 in Fig. 4 are removed and antenna #4 is fed at the same position on the y-coordinate.

Figure 20 shows $S21$s of the 5-element model (Fig. 4) and the 3-element model (Fig. 19). The position of the antenna sensor is $x = 0$ mm. $S21$ is normalized by each maximum value. The received waves from the blood vessel are observed at around 0.23 and 0.35 ns in both models. However, the received wave in the 3-element model is 1.5 times bigger than that of the 5-element model. This might be due to the fact that since the mutual coupling between transmitting antenna #1 and receiving antennas #3 and #5 is removed, receiving antenna #2 becomes more sensitive to the blood vessel.

Figure 21 shows the simulated amplitudes of the transmission coefficients in the case that the antenna sensor is moved from $x = -20$ to $+20$ mm. The amplitude between -0.15 and 0.15 is shown in a color gradation image in $h_b = 5$ mm. The amplitude between -0.08 and 0.08 is shown in a color gradation image in $h_b = 10$ mm. The final antenna sensor is used. The images can be observed at 0.23 ns in $h_b = 5$ mm and at 0.35 ns in $h_b = 10$ mm. The positions
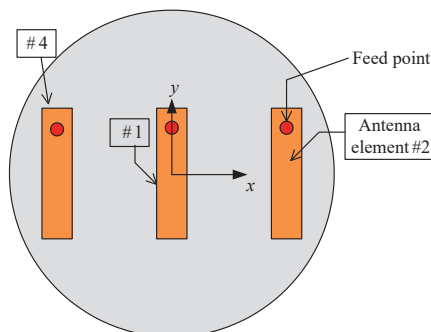
Fig. 19. (Color online) Geometry of the final antenna sensor (3-element model).
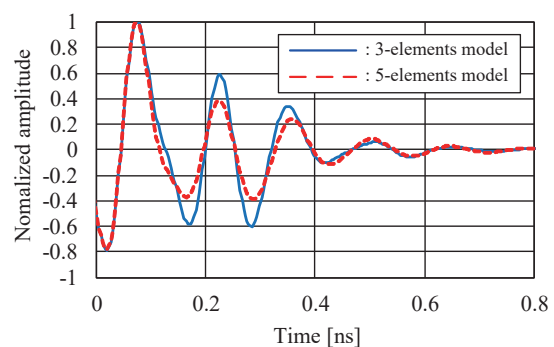
Fig. 20. (Color online) $S21$s in 5- and 3-element models.
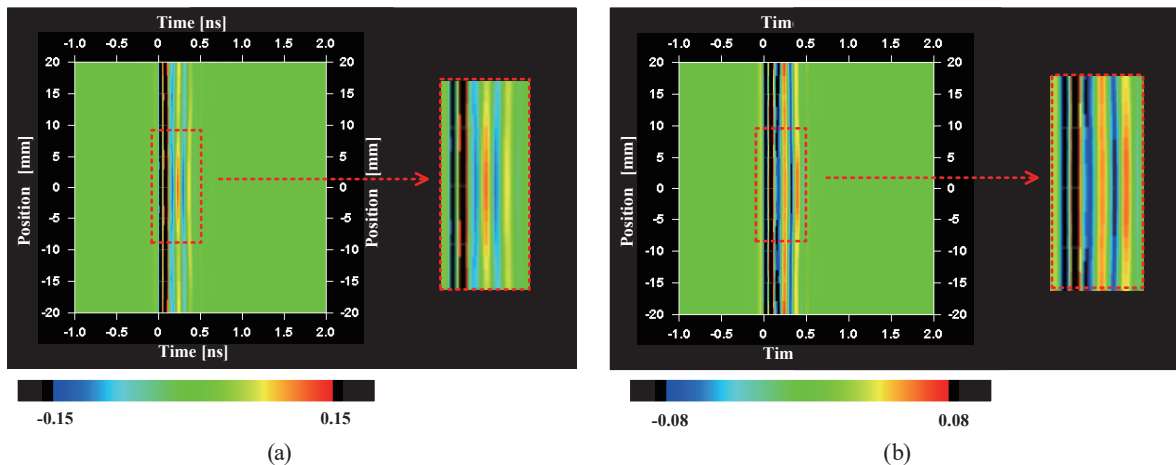
Fig. 21.   (Color) Simulated amplitudes of transmission coefficients when the antenna sensor is moved from $x = -20$ to $+20$ mm.   (a) $h_b = 5.0$ mm and (b) $h_b = 10.0$ mm.

of the image of the blood vessel deviate from that of the actual blood vessel in the 5-element model.   However, the blood vessel exists symmetrically to $x = 0$ mm in the 3-element model. The position of the blood vessel up to $h_b = 10$ mm is accurately detected by feeding receiving antennas #2 and #4 at the same edge side and averaging the amplitudes of the transmission coefficients $S21$ and $S41$.

Figures 22(a) and 22(b) show $S21$ between the antenna positions $x = 0$ and $+20$ mm. $S21$ is normalized by each maximum value.   At 0.23 ns in $x = 0$ mm, the ratio of the receiving wave to the direct wave is 0.4 in $h_b = 5$ mm and 0.5 in $h_b = 10$ mm.   At 0.35 ns in $x = 0$ mm, the ratio of the receiving wave to the direct wave is 0.21 in $h_b = 5$ mm and 0.18 in $h_b = 10$ mm.   The reception level from the blood vessel for the direct wave is greater than −15 dB (0.18).   The direct wave is estimated to be approximately −30 dB at 8 GHz from Fig. 7.   Therefore, the reception level for the input power at the feed point of the antenna is −45 dB (= −15–30 dB). The designed antenna sensor satisfies the specification (−60 dB) of the reception level.   When the position of the blood vessel is shallow ($h_b = 5$ mm), the difference in magnitude between the signal reflected from the blood vessel and the signal in the case without the blood vessel is large at 0.23 ns.   When the position of the blood vessel is deep ($h_b = 10$ mm), the difference in the arrival time between the signal reflected from the blood vessel and the signal in the case without the blood vessel is large at around 0.35 ns.   For these reasons, the image of the blood vessel is observed at $h_b = 5$ and 10 mm, as shown in Fig. 21.

Noise is not considered in the simulation in this study.   However, noise will occur in the measured data.   The waves reflected from objects other than the blood vessel and the higher harmonic noise components are the expected types of noise.   Such noise can be removed by installing a time domain filter and a frequency domain filter.
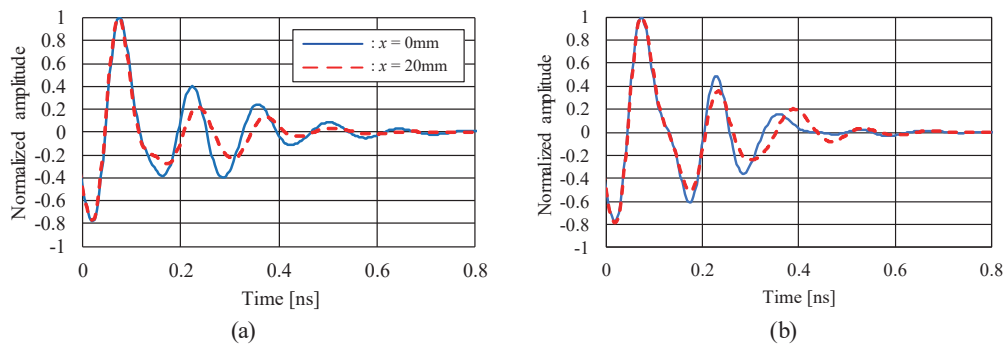
Fig. 22. (Color online) $S21$ between the antenna positions $x = 0$ and $+20$ mm. (a) $h_b = 5.0$ mm and (b) $h_b = 10.0$ mm.

5. Conclusions

In this paper, the radio-wave-type endoscope has been proposed and the antenna sensor for the endoscope was designed by simulation. As the first step of our study, the proposed antenna sensor was examined in a 2.5-times scale model to facilitate the fabrication and measurement of the antenna sensor. A microstrip antenna was used as the antenna element. In the simulation, it was confirmed that a blood vessel of 10 mm diameter could be detected at a distance of 10 mm from the top surface of the fatty tissue in the 2.5-times scale model using the designed antenna sensor.

In order to evaluate the feasibility and effectiveness of the proposed antenna sensor, it is necessary to verify the simulated results in a measurement experiment. We plan to conduct the experiment using phantoms of fatty tissue and blood vessels.

Acknowledgments

References

1 R. Oguma, T. Nakaguchi, R.Nakamura, T. Yamaguchi, H. Kawahira, and H. Haneishi: Med. Imaging Technol. **32** (2014) 203.
2 J. Kaneko, H. Kudo, A. Miyata, S. Yamamoto, J. Arita, N. Akamatsu, K. Hasegawa, Y. Sugawara, and N. Kokudo: MEDIX **62** (2015) 4.
3 Y. Hayakawa, H. Yamashita, T. Otsuburai, Y. Miyoseta, M. Sagawa, A. Kondo, Y. Tsuji, and A. Honda: Med. Imaging Inf. Sci. **27** (2010) 50.
4 J. Bourqui, M. Okoniewski, and E. C. Fear: IEEE Trans. Antennas Propag. **58** (2010) 2318.
5 M. Serhir and D. Lesselier: IEEE Trans. Antennas Propag. **66** (2018) 1056.
6 C. A. Balanis: Antenna Theory (Wiley, New York, 1997) 2nd ed., Chap. 14.
7 REMCOM: https://www.remcom.com/xfdtd-3d-em-simulation-software/ (accessed March 2017).
8 G. Sinclair : Proc. THE I.R.E (1948) 1364–1370.
9 IFAC: http://niremf.ifac.cnr.it/tissprop/htmlclie/htmlclie.php (accessed March 2017).

About the Authors

Takafumi Fujimoto received his B.E. and M.E. degrees from Nagasaki University, Japan, in 1992 and 1994, respectively, and a Dr.Eng. degree from Kyushu University, Japan, in 2003. He is currently an associate professor at Nagasaki University. From November 2004 to September 2005, he was a visiting scholar in the Department of Electrical and Computer Engineering, University of Illinois at Urbana-Champaign. His main interests are in the analytical method and design of printed antennas in antenna engineering and diffraction-free beams in optical engineering. He is a member of the Institute of Electrical and Electronics Engineers (IEEE), Institute of Electronics, Information and Communication Engineers (IEICE), Institute of Image Information and Television Engineers ITE), and Optical Society of America (OSA).

Keiya Kawashima received his B.S. degree from Nagasaki University, Japan, in 2017. He is currently a student at the Graduate School of Engineering, Nagasaki University. His research interest is in antenna design. He is a student member of the Institute of Electronics, Information and Communication Engineers (IEICE).

Genki Horiguchi received his B.S. degree from Nagasaki University, Japan, in 2017. He is currently a student at the Graduate School of Engineering, Nagasaki University. His research interest is in the development of exploration equipment using electromagnetic waves. He is a student member of the Institute of Electronics, Information and Communication Engineers (IEICE).

Toshiyuki Tanaka received his B.E. degree from Nagasaki University, Japan, in 1984 and his M.E. and D.E. degrees from Kyushu University, Japan, in 1986 and 1989, respectively. From 1989 to 1993, he was an assistant professor at Nagasaki University, Japan. Since 1993, he has been an associate professor at Nagasaki University. His research interests are in the development of a nondestructive inspection device and a noninvasive diagnostic device using electromagnetic waves. He is a member of the Institute of Electronics, Information and Communication Engineers (IEICE), Institute of Electrical Engineers of Japan (IEEJ), and Japan Concrete Institute (JCI).